Journal of Materials Chemistry C

ROYAL SOCIETY OF CHEMISTRY

PAPER

View Article Online
View Journal | View Issue

Cite this: J. Mater. Chem. C, 2026, 14, 3181

Fabrication of 3D PEDOT:PSS composite microstructures *via* two-photon polymerisation

Jason M. Delente, *[a] Srikanth Kolagatla,[a] Naroa Lopez-Larrea,[b] Miryam Criado-Gonzalez,[bc] Marco Carlotti,[de] Brian J. Rodriguez,[f] Colm Delaney,[a] David Mecerreyes,[bg] Virgilio Mattoli[d] and Larisa Florea *[a]

Received 6th August 2025,
Accepted 14th December 2025

DOI: 10.1039/d5tc02981c

rsc.li/materials-c

Two-photon polymerisation is a cutting-edge fabrication technique that enables the creation of complex 3D polymer microstructures. The miniaturisation of electronics, enabling advances in micro-robotics and discreet monitoring systems necessitates the production of conductive microstructures. Herein, two photoresist formulations containing poly(3,4-ethylenedioxythiophene) doped with poly(styrene sulfonate) (PEDOT:PSS) are proposed for fabricating microstructures *via* two photon polymerisation. An in-depth characterisation of the resulting microstructures and their composition are presented using Raman spectroscopy, scanning electron microscopy and atomic force microscopy. Additionally, the conductivity of the microstructures is further analysed through conductive atomic force microscopy (C-AFM), and Kelvin probe force microscopy (KPFM).

Introduction

Conductive gels have emerged as a compelling alternative to conventional rigid electronics in developing conformable electronic devices.[1–4] Various methods have been used to develop conductive hydrogels, the most common being composite materials comprising insulating polymers and conducting constituents, ranging from carbon nanotubes,[5–9] graphene,[10–13] inorganic nanoparticles/nanowires,[14–16] and conductive polymers.[17,18] Among them, conducting polymer hydrogels have proven extremely versatile for biomedical applications and conformable electronics.[17,19–21] Poly(3,4-ethylenedioxythiophene) doped with poly(styrenesulfonate) (PEDOT:PSS) has been extensively studied due to its biocompatibility, thermal and electrical stability, and high conductivity.[22,23] However, it remains challenging to formulate highly conductive hydrogels containing PEDOT:PSS due to its limited solubility and the need for additional components to form hydrogels. This often results in a trade-off between the processability of the hydrogel and its mechanical and conductive properties.[24]

Recently, various additive manufacturing techniques have been used to fabricate PEDOT-based 3D conductive hydrogels, such as inkjet printing,[25,26] extrusion-based printing,[21,27,28] and light-based printing.[29] While these methods have a resolution that is limited to tens of micrometres,[30] direct laser writing (DLW) by two-photon polymerisation (TPP) is the technology of choice for the generation of sophisticated 3D architectures at the microscale, with high-aspect ratios. It has been exploited in very diverse areas of research such as micro-robotics,[31,32] fabrication of photonic structures,[33–35] sensors,[36–38] micro-optics,[39,40] thermo-responsive actuators,[41,42] pH-responsive actuators,[43,44] and cellular scaffolds.[45,46]

The miniaturisation of electronics has driven interest in the fabrication of microscale conductive patterns, thus the use of two-photon absorption (TPA) to form metallic patterns (zinc, silver, platinum, palladium, and gold) has been explored and is showing promising results.[47–51] Despite demonstrating excellent conductivity, the metallic micropatterns are often limited to 2D/2.5D without the possibility of fine tuning the Young's modulus of the material. Therefore, the use of organic conducting polymers, allowing for the tunability of moduli for the desired application and improved biocompatibility is also being investigated.

To date, few examples of TPP fabrication of electrically conductive PEDOT:PSS containing polymeric microstructures have been reported, of which the conductivity was compiled in a recent review.[52] Particular interest has been drawn to the use of multistep approaches with post-fabrication modification of

[a] School of Chemistry & AMBER, The SFI Research Centre for Advanced Materials and BioEngineering Research, Trinity College Dublin, Dublin 2, Ireland. E-mail: delentej@tcd.ie, floreal@tcd.ie
[b] POLYMAT University of the Basque Country UPV/EHU, Avenida de Tolosa 72, 20018 Donostia-San Sebastián, Spain
[c] Institute of Polymer Science and Technology, CSIC, C/Juan de la Cierva 3, 28006 Madrid, Spain
[d] Center for Materials Interfaces, Istituto Italiano di Tecnologia, Via R. Piaggio 34, 56025 Pontedera, Italy
[e] Dipartimento di Chimica e Chimica Industriale, University of Pisa, Via Moruzzi 13, 56124 Pisa, Italy
[f] School of Physics and Conway Institute of Biomolecular and Biomedical Research, University College Dublin, Belfield, Dublin, D04 V1W8, Ireland
[g] Ikerbasque, Basque Foundation for Science, 48013 Bilbao, Spain

the microstructures either by adsorption of PEDOT,[53] or by the oxidative polymerisation of EDOT, achieving a conductivity of 0.04 S cm^{-1}.[54] The possibility to fabricate microstructures directly with PEDOT:PSS within the photoresist *via* TPP was only recently demonstrated. For example, PEDOT:PSS pellets were dissolved in IPA and mixed with the commercially available acrylate-based photoresin IP-L.[55] Importantly, a conductivity of 3.5 × 10^2 S cm^{-1} was measured for the fabricated structures that could further be used as humidity sensors. On the other hand, the most common approach involves using a commercially available PEDOT:PSS dispersion.[56] The highest content of PEDOT:PSS used for TPP was recently achieved by Lichade *et al.* who fabricated conductive microstructures using a photoresist containing 88 wt% of commercially available PEDOT:PSS suspension in combination with poly(ethylene oxide), achieving a resistance of 410 Ω; however, these results came with the trade-off of limited possibilities for the fabrication of 3D structures.[57] Therefore, there is a need for the expansion of photoresists that incorporate a high quantity of conducting polymers such as PEDOT:PSS for the fabrication of complex 3D conductive microstructures for a wider range of applications while maintaining high resolution for fabrication and enabling control over the mechanical properties of the resulting structures.

Herein, two photoresist formulations containing a content of commercially available PEDOT:PSS suspension (≈58 wt%) that is one of the highest reported, were investigated along with their use for the TPP fabrication of high-aspect ratio complex 3D microstructures (Fig. 1). Then, an extensive characterisation of the TPP printed microstructures is outlined, detailing the study of the chemical composition of microstructures by Raman spectroscopy, and of their morphology using scanning electron microscopy (SEM) and atomic force microscopy (AFM). Furthermore, an in-depth study of both their mechanical and conductive properties using AFM, conductive atomic force microscopy (C-AFM), and kelvin probe force microscopy (KPFM) is performed to fully characterise the properties of these miniaturised electronic materials at the microscale.

Experimental section

Materials and instruments

Trimethylolpropane ethoxylate triacrylate (M_n ~ 912 g mol^{-1}; TMPET-912), poly(ethylene glycol) diacrylate (M_n ~ 700 g mol^{-1} PEGDA-700), ethylene glycol, lithium phenyl(2,4,6-trimethylbenzoyl)phosphinate (LAP) were purchased from Sigma-Aldrich, Merck, Hach, and TCI Chemicals, were of reagent grade, and were used as received. PEDOT:PSS suspension Clevios PH1000 grade (containing 1.3 wt% of solid PEDOT:PSS content) was purchased from Heraeus Epurio and was sonicated for 1 hour before use. In the following photoresist compositions, the weight percentage of Clevios PH1000 used in the formulation is indicated in the name of the photoresist. The actual content of PEDOT:PSS and water are described separately in the tables.

Preparation of photoresists

Crosslinkers and ethylene glycol were mixed in a glass vial before the addition of the desired quantity of Clevios PH1000. The dispersion was mixed for a further 30 seconds using a

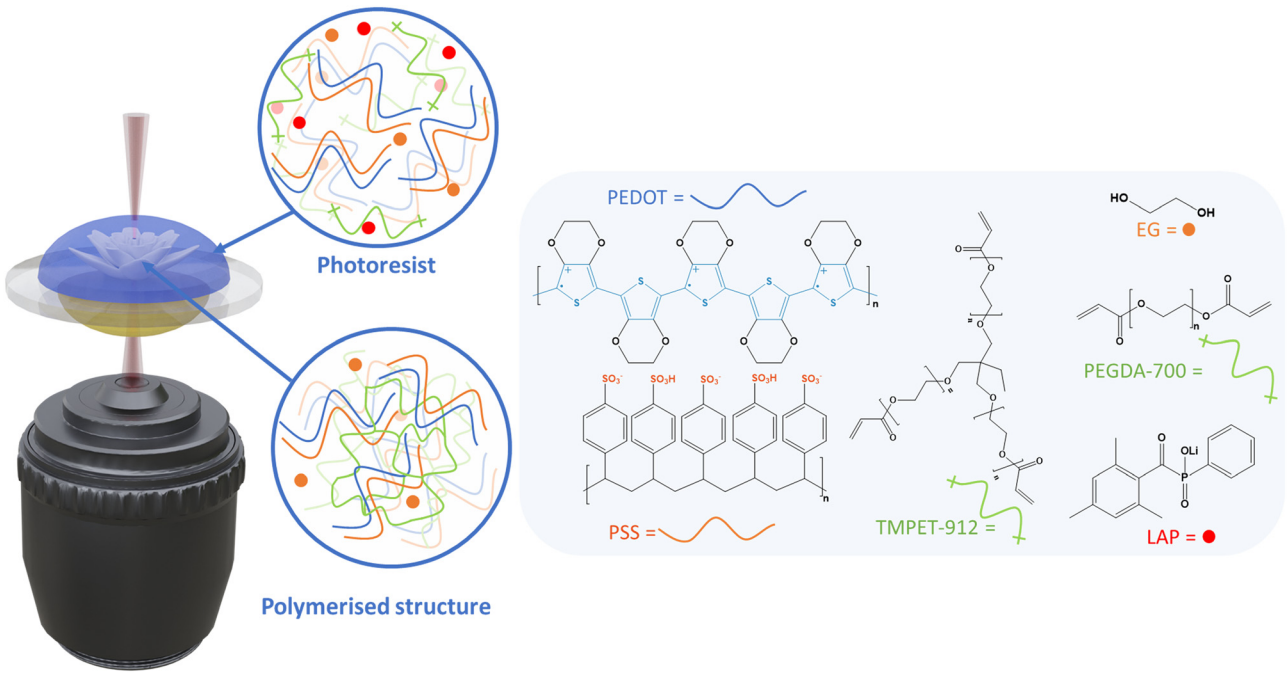

Fig. 1 Scheme of two-photon polymerisation in oil immersion configuration for the fabrication of microstructures, and components of the photoresist: poly(3,4-ethylene dioxythiophene):poly(stryrenesulfonate) (PEDOT:PSS), ethylene glycol (EG), poly(ethylene glycol) diacrylate M_n = 700 g mol^{-1} (PEGDA-700), trimethylolpropane ethoxylate triacrylate M_n = 912 g mol^{-1} (TMPET-912), lithium phenyl-2,4,6-trimethylbenzoylphosphinate (LAP). Presence of a coverslip on top of the photoresist was omitted for clarity.

Table 1 Composition of photoresist 1 – PEGDA, 57.8 wt% Clevios

Chemical	Quantity (mg)	Weight%
PEDOT:PSS	6.5	0.75
PEGDA-700	305.0	35.30
Ethylene glycol	20.0	2.30
LAP	40.0	4.60
Water	493.5	57.05

Table 2 Composition of photoresist 2 – PEGDA/TMPET, 58.3 wt% Clevios

Chemical	Quantity (mg)	Weight%
PEDOT:PSS	13	0.76
PEGDA-700	400	23.32
TMPET-912	200	11.67
Ethylene glycol	40	2.33
LAP	75	4.37
Water	987	57.55

vortex mixer, followed by the addition of LAP photoinitiator. The mixture was stirred for a few hours at 25 °C before being used. The exact compositions of photoresists 1 – PEGDA, 57.8 wt% Clevios and 2 – PEGDA/TMPET, 58.3 wt% Clevios are shown in Tables 1 and 2, respectively.

Direct laser writing fabrication

A commercial direct laser writing (DLW) workstation, Photonic Professional Nanoscribe GmbH, was used for the fabrication of the 3D structures *via* two-photon polymerisation using the photoresist formulations indicated in Tables 1 and 2. The system operates at a wavelength of 780 nm, using a 50 mW femtosecond solid–state laser that delivers 120 fs pulses with an 80 MHz ± 1 MHz repetition rate. An oil-immersion configuration was employed, using a 63× immersion objective (NA = 1.4, WD = 190 μm) (Zeiss, Plan Apochromat). Sample positioning was controlled by a 3D galvo translation stage.

To begin the fabrication process, a single drop of the photoresist (blue dome in Fig. 1) was placed on the centre of the silanised glass slide and the photoresist was slowly evaporated at room temperature for 30 minutes before placing a cover slide on the top. A drop of oil (Zeiss Immersol 518F) was placed in the centre of the opposite side of the glass substrate (shown in Fig. 1). During the fabrication process, the scan speed and the laser power were varied to achieve optimised printing. Once the fabrication process was complete, structures were carefully developed in water : 2-propanol (70 : 30) followed by 2-propanol to remove residual unpolymerised photoresist.

Experimental details and conditions are presented in the SI.

Results and discussion

Photopolymerisation kinetics of bulk photoresist formulations

Bulk photopolymerisation of the two photoresist formulations was studied by photorheology in order to investigate their photo-curing behaviour. Before irradiation, the loss modulus (G'') presented higher values than the storage modulus (G'), which is a signature of the solution-like state of the inks. After 60 s, the UV light was switched on (λ_{ex} = 365 nm, power 1 mW cm^{-2}) leading to a rapid increase of G', which surpassed G'', corroborating the gel formation in less than 8 seconds of UV exposure in both cases (Fig. S1, SI). The expected mechanism of polymerisation was further evidenced by the disappearance of the band located at 980 cm^{-1}, which corresponds to the C=C bending out of plane, in the infrared spectra.

Direct laser writing of PEDOT:PSS containing microstructures

The commercially available PEDOT:PSS aqueous dispersion used in the preparation of all the photoresists is known as Clevios PH1000 and contains 1.3 wt% of solid PEDOT:PSS content. Ethylene glycol, the crosslinker PEGDA-700 or the 2 : 3 mixture of PEGDA-700 : TMPET-912 was mixed with PEDOT:PSS before the addition of the water-soluble photoinitiator LAP. Absolute concentration of the crosslinkers plays an important role in polymerisation parameters. DLW in small volumes of photoresist in open-cells can be prone to evaporation of solvent. This is demonstrated in Fig. S2, SI. Therefore, as described in the Experimental section, the photoresist was deposited on the silanised surface of the substrate, and a settling time of 30 min was implemented, leading to evaporation and a slight gelation of the photoresist. This was followed by the addition of a coverslip on the top of the photoresist to avoid further evaporation once an optimal water content was reached, thus enabling the fabrication of microstructures by DLW. The water evaporation was quantified to 16.9 ± 1.55% and 15.9 ± 1.67% of the initial weight for photoresists 1 – PEGDA, 57.8 wt% Clevios, and 2 – PEGDA/TMPET, 58.3 wt% Clevios, respectively (Tables S1 and S2, SI)

Since two-photon absorption is a nonlinear process, the probability of absorption is dependent on the square of the intensity of the light, which limits the polymerisation reaction to the focal point of the laser, representing a volume of a few hundred nanometers called a voxel.[58] This can be exploited to generate small and intricate features. SEM images of a selection of 3D microstructures fabricated using the photoresists 1 – PEGDA, 57.8 wt% Clevios, and 2 – PEGDA/TMPET, 58.3 wt% Clevios are shown in Fig. 2 and SI (Fig. S3, S4). Thus, demonstrating the ability to fabricate 3D structures with both photoresists precisely, containing overhanging features, and resolution between features. For example, the woodpile microstructure shows minimum feature sizes of 698 ± 64 nm and 1018 ± 78 nm in *X*–*Y* directions, for photoresists 1 – PEGDA, 57.8 wt% Clevios, and 2 – PEGDA/TMPET, 58.3 wt% Clevios, respectively (Fig. 2) revealed through SEM analysis.

Arrays of cubes with dimensions of 50 × 50 × 30 μm were fabricated and used for characterisation by Raman spectroscopy along the pre-polymer analogues. The fingerprint of PEDOT was visible for both photoresists, notably with a strong peak at 1430 cm^{-1} accounting for C_α=C_β stretching and at 1508 cm^{-1} for C_α=C_β asymmetric stretching (Fig. 3).[59] The peaks at 1641 and 1637 cm^{-1} corresponding to C=C vibration of the crosslinkers for photoresists 1 – PEGDA, 57.8 wt% Clevios, and 2 – PEGDA/TMPET, 58.3 wt% Clevios, respectively, are not present in the spectra measured on the structures

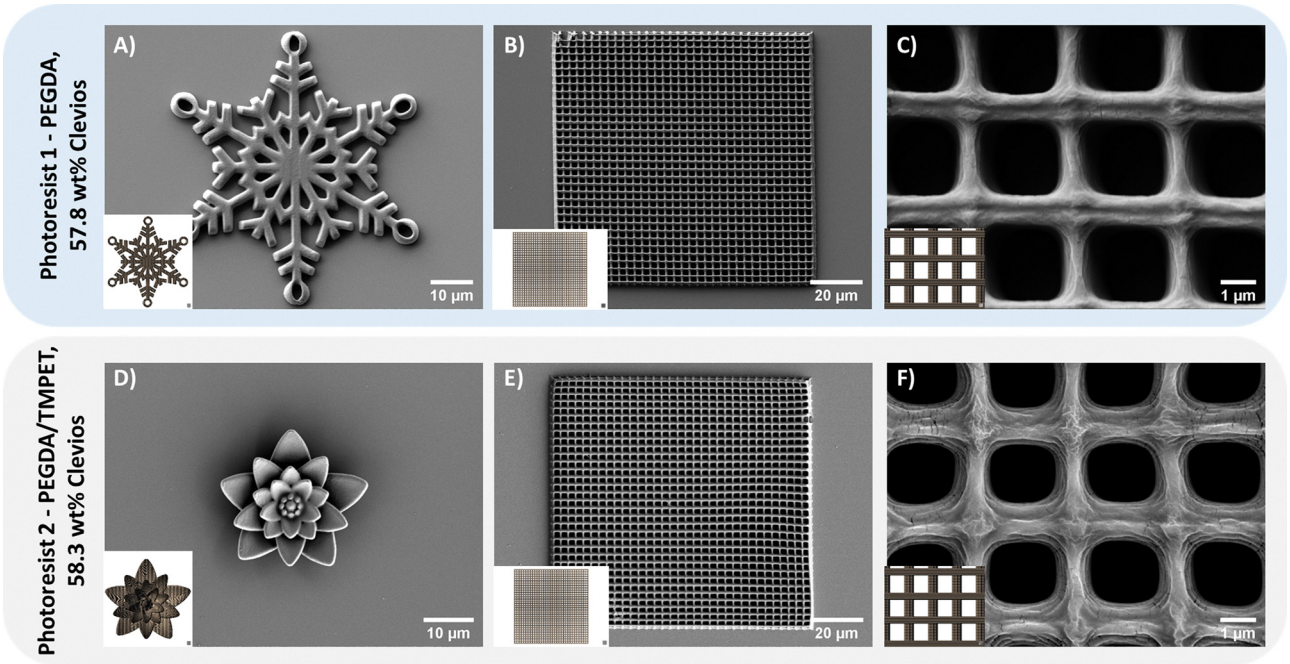

Fig. 2 SEM pictures of structures fabricated using photoresist 1 – PEGDA, 57.8 wt% Clevios including (A) snowflake, (B) woodpiles with 5 layers and (C) higher magnification of (B), and using photoresist 2 – PEGDA/TMPET, 58.3 wt% Clevios including (D) Water lily, (E) woodpiles with 5 layers and (F) higher magnification of (E). Scale bar representing 10 µm for (A) and (D), 20 µm for (B) and (E), 1 µm for (C) and (F).

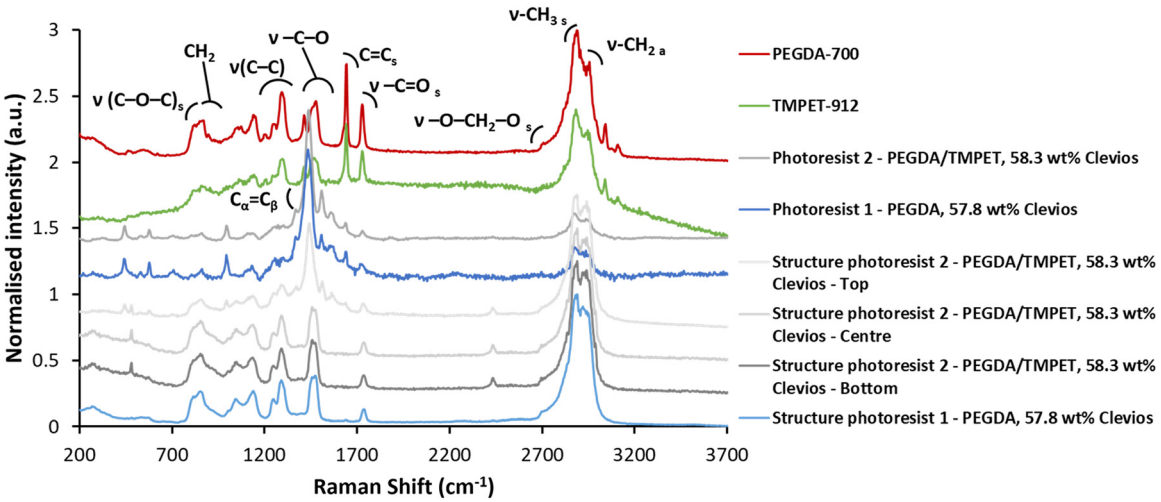

Fig. 3 (A) Raman spectra of PEGDA-700, TMPET-912, photoresist 1 – PEGDA, 57.8 wt% Clevios and photoresist 2 – PEGDA/TMPET, 58.3 wt% Clevios, and cubes (50 × 50 × 30 µm) fabricated by TPP using photoresist 1 – PEGDA, 57.8 wt% Clevios, and photoresist 2 – PEGDA/TMPET, 58.3 wt% Clevios.

fabricated by TPP, thus confirming the polymerisation.[60] Spectra of the microstructures fabricated with photoresists 1 – PEGDA, 57.8 wt% Clevios, and 2 – PEGDA/TMPET, 58.3 wt% Clevios displayed similar peak to their corresponding crosslinker components, with the peak at 2929 cm^{-1} representing the $–CH_2$ asymmetric stretching, the peak at 2885 cm^{-1} corresponding to $–CH_3$ symmetric stretching and the shoulder at 2720 cm^{-1} accounting for the symmetric stretching of C–H for a $–O–CH_2–O$ system. A weak band at 1737 cm^{-1} corresponds to the stretching of the carbonyl bond, and the bands at 1292 and 1247 cm^{-1} account for the C–O stretch of the ester moieties, while the band at 1045 cm^{-1} corresponds to the C–C stretch of the backbone.[61,62] Analysis using Raman spectroscopy revealed that the signal of PEDOT within the structure is masked by the signals corresponding to the crosslinkers, presumably due to the low concentration of PEDOT. Indeed, structures fabricated using photoresists 1 – PEGDA, 57.8 wt% Clevios, and 2 – PEGDA/TMPET, 58.3 wt% Clevios displayed similar bands to the ones of photoresist 3 – PEGDA, 57.8 wt% water (same composition as photoresist 1 – PEGDA, 57.8 wt% Clevios but the commercial PEDOT:PSS dispersion was replaced by

DI water Table S3 and Fig. S5, SI). Interestingly, when focusing on the top part of one of the structures, the Raman spectra significantly changed to display one of the characteristic peaks of the Raman spectra of PEDOT with a strong peak at 1444 cm^{-1} accounting for $C_\alpha{=}C_\beta$ stretching.[63]

Atomic force microscopy characterisation of mechanical properties of microstructures

The swelling and mechanical properties of the microstructures fabricated using photoresists 1 – PEGDA, 57.8 wt% Clevios, and 2 – PEGDA/TMPET, 58.3 wt% Clevios were investigated using atomic force microscopy (AFM, Fig. 4). Arrays of cuboid structures 10 × 10 × 4 μm were fabricated with laser power ranging from 25 mW to 36.5 mW for photoresist 1 – PEGDA, 57.8 wt% Clevios and from 15 mW to 22 mW for photoresist 2 – PEGDA/TMPET, 58.3 wt% Clevios. As seen in Fig. 4A, the structures fabricated using photoresist 1 – PEGDA, 57.8 wt% Clevios varied in height from 3.20 ± 0.06 μm to 3.63 ± 0.03 μm in dry state, swelling to 4.48 ± 0.04 μm to 5.05 ± 0.06 μm in water, respectively, thus demonstrating a constant swelling of 40% from their dehydrated form. The structures fabricated using photoresist 2 – PEGDA/TMPET, 58.3 wt% Clevios varied in height from 3.20 ± 0.12 μm to 3.60 ± 0.03 μm in dry state, swelling to 3.64 ± 0.03 μm to 4.40 ± 0.04 μm in water, respectively, thus demonstrating a swelling ranging from 13 to 22% from their dehydrated form. This demonstrates the influence of the crosslinker on the structures' ability to swell in aqueous solution. As expected, the more crosslinked hydrogel microcubes showed less swelling.

Young's modulus measurements were also performed on the microcubes. For photoresist 1 – PEGDA, 57.8 wt% Clevios, a range of moduli from 32.46 ± 0.38 to 48.53 ± 0.36 MPa was measured in air, reducing to 7.44 ± 0.12 to 9.01 ± 0.52 MPa in water (Fig. 4B). While the Young's modulus value for structures fabricated with photoresist 2 – PEGDA/TMPET, 58.31 wt% Clevios in air ranged from 44.52 ± 16.16 to 73.09 ± 1.37 MPa and from 10.27 ± 0.98 to 18.32 ± 0.36 MPa in water. The modulus values for both samples increased with increasing laser power. This is expected due to an increase in the crosslinking density of the network with increased laser dosage. In the aqueous solution, the cubes hydrated as seen from AFM height measurements and became softer, as observed from the decrease in Young's modulus values for hydrated samples. Moreover, the Young's modulus increase recorded for the hydrogel microcubes fabricated with photoresist 2 – PEGDA/TMPET, 58.31 wt% Clevios, compared to photoresist 1 – PEGDA, 57.8 wt% Clevios, corresponds to the more crosslinked network, in agreement with the swelling tests. Overall, the AFM results showed that the fabricated structures are soft in nature but retain their integrity after hydration, showing their mechanical stability. The Young's modulus values determined for the hydrated microcubes are of the same order of magnitude as those determined for the macrogels prepared with photoresists 1 – PEGDA, 57.8 wt% Clevios, and 2 – PEGDA/TMPET, 58.31 wt% Clevios (Fig. S6, SI).

Conductive properties of the microstructures

Conductive properties of 3 μm tall microstructures were studied. The current response of structures fabricated on top of ITO electrodes, was characterised *via* conductive-AFM (Fig. 5A and Fig. S7–S9, SI). Upon application of a 1 V bias, a current response of 3 pA was measured for photoresist 1 – PEGDA, 57.8 wt% Clevios. To study the effect of the concentration of PEDOT:PSS on the conductivity of the microstructures, photoresist 4 – PEGDA, 20 wt% Clevios (composition shown in Table S4, SI) was formulated with a lower concentration of PEDOT:PSS (20 wt%) than photoresist 1 – PEGDA, 57.8 wt% Clevios. A lowered current response 2.5 pA was observed on structures fabricated using photoresist 4 – PEGDA, 20 wt% Clevios (Fig. S7C and S8C, SI). The *I–V* plots for the structure fabricated using photoresist 1 – PEGDA, 57.8 wt% Clevios showed that the maximum current at −5 V bias is −42 pA on top of the structure (Fig. S9, SI), against −25 pA on top of the structure fabricated using photoresist 4 – PEGDA, 20 wt% Clevios (Fig. S7–S9, SI). The C-AFM measurements on both samples demonstrated that an increase in PEDOT concentration led to an increase in the current response.

Additionally, the effect of PEDOT:PSS on the conductive properties of the structures fabricated using photoresist 1 – PEGDA, 57.8 wt% Clevios, and photoresist 2 – PEGDA/TMPET, 58.31 wt% Clevios was further confirmed with C-AFM

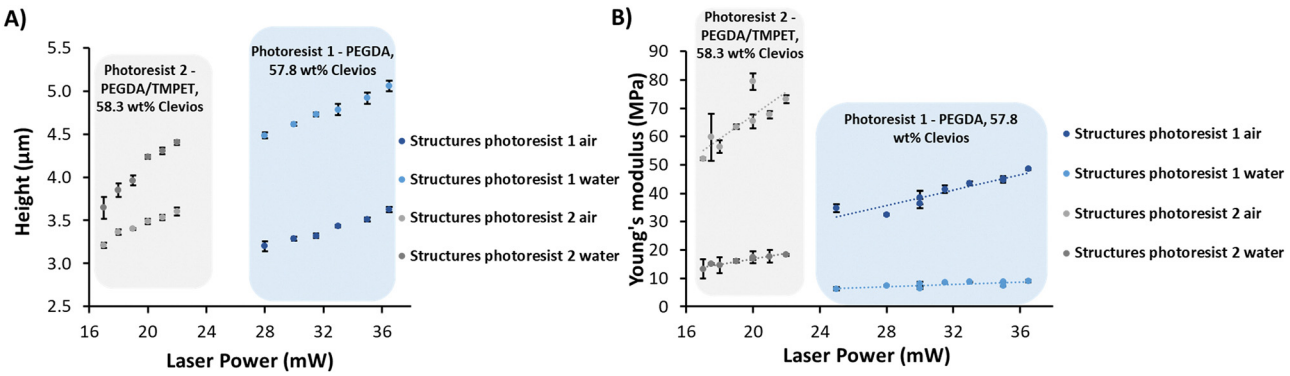

Fig. 4 AFM (A) height and (B) Young's modulus measurements of the micro-cubes fabricated using photoresist 1 – PEGDA, 57.8 wt% Clevios, and photoresist 2 – PEGDA/TMPET, 58.3 wt% Clevios in air and water at various laser power.

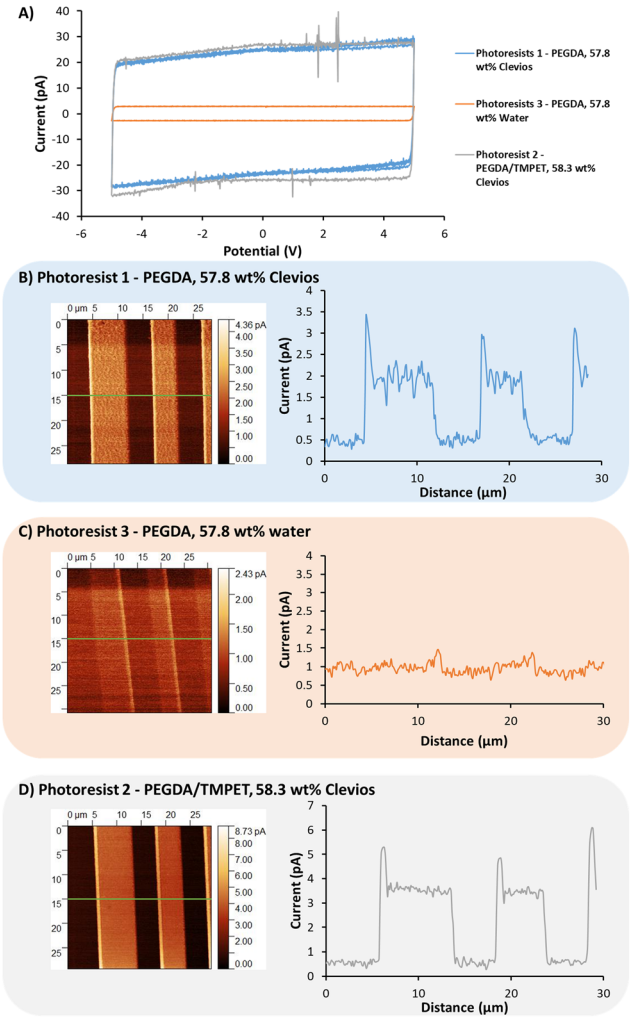

Fig. 5 (A) C-AFM I-V curves current measurements on structures fabricated using photoresists 1 – PEGDA, 57.8 wt% Clevios, 3 – PEGDA, 57.8 wt% water, and 2 – PEGDA/TMPET, 58.3 wt% Clevios. (B), (C) and (D) Current images (left) and current response (right) measured when scanning the structures upon applying a bias of 4 V for structures fabricated using the photoresists 1 – PEGDA, 57.8 wt% Clevios, 3 – PEGDA, 57.8 wt% water, and 2 – PEGDA/TMPET, 58.3 wt% Clevios, respectively. The green lines represent the scanning paths.

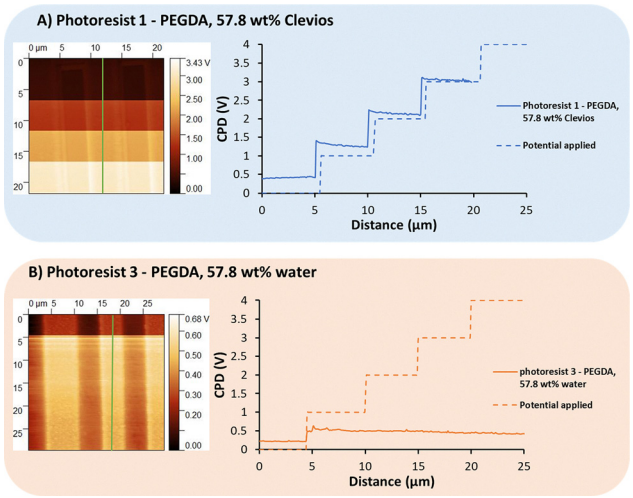

Fig. 6 (A) and (B) Images of the linear structures used for KPFM experiment with the substrate bias (left), fabricated using photoresists 1 – PEGDA, 57.8 wt% Clevios, and 3 – PEGDA, 57.8 wt% water, respectively. The green lines represent the scanning paths. Plots of the contact potential difference in the function of the bias applied to the structures (right).

measurements carried out on grid-like structures. A response of approximately 30 pA was measured for both structures fabricated with photoresists 1 – PEGDA, 57.8 wt% Clevios, and 2 – PEGDA/TMPET, 58.31 wt% Clevios, and a clear variation in conductivity was observed when scanning the structure followed by the substrates (Fig. 5). As seen in Fig. 5A, no current response was observed on the IV plot of the structures fabricated using photoresist 3 – PEGDA, 57.8 wt% water, and no difference was observed when scanning alternatively the structure and the glass substrate (Fig. 5C).

The structures fabricated with photoresist 1 – PEGDA, 57.8 wt% were further characterised using Kelvin probe force microscopy (KPFM), which is used to study the surface properties of conductive samples.[64] KPFM is also used to determine the work function of materials, which corresponds to the minimum energy needed to move electrons at the Fermi level, and is characteristic of the conductive material. The calculated work function of the structure was 4.98 eV while the literature value for PEDOT:PSS was 5 eV.[65] Therefore, the conductivity arising from the structure can be attributed to the presence of PEDOT:PSS. Furthermore, when increasing the bias applied to the sample, a contact potential difference response of the equivalent bias could be measured (Fig. 6). A similar result was observed when characterising structures fabricated with the photoresist 2 – PEGDA/TMPET, 58.31 wt% Clevios (Fig. S10, SI). When carrying out the same experiment with structures fabricated using the photoresist 3 – PEGDA, 57.8 wt% water, a response of 3 pA could be measured when applying a bias of 4 V, while when increasing the bias applied to the structure no contact potential difference could be observed (Fig. 6B), which further demonstrated that there is conduction of electrons through the structures fabricated using photoresists 1 – PEGDA, 57.8 wt% Clevios, and 2 – PEGDA/TMPET, 58.31 wt% Clevios.

Additionally, cylinders of 850 µm thickness and a diameter of 10 mm were fabricated using photoresists 1 – PEGDA, 57.8 wt% Clevios, and 2 – PEGDA/TMPET, 58.31 wt% Clevios *via* bulk exposure to UV light (λ = 365 nm) to characterise the conductive properties of the macroscale samples. A conductivity of 3×10^{-3} ($\pm 1 \times 10^{-3}$) and 2×10^{-3} ($\pm 1 \times 10^{-3}$) S cm^{-1} was obtained for the cylinders fabricated with photoresists 1 – PEGDA, 57.8 wt% Clevios, and 2 – PEGDA/TMPET, 58.31 wt% Clevios, respectively, as determined with the four-point probe technique (Fig. S11, SI). Besides, cyclic voltammograms showed a proportional increase of both the anodic and cathodic currents with the scan rate. It demonstrates that the redox reactions are not limited by the rate of diffusion of ions or electrons within the hydrogel and that all the redox active

species within the hydrogel are participating not just the ones at the surface (Fig. S11, SI).

Conclusions

This study presented two photoresist formulations containing a high weight percentage of a commercially available PEDOT:PSS aqueous dispersion Clevios PH1000. These formulations demonstrated successful fabrication of 3D microstructures *via* direct laser writing with a minimum feature size of 700 nm for photoresist 1 – PEGDA, 57.8 wt% Clevios and 1 μm for photoresist 2 – PEGDA/TMPET, 58.31 wt% Clevios, under the current experimental conditions. Importantly, this work fully characterised the resulting materials at the microscale using atomic force microscopy. The mechanical properties of microstructures fabricated with the two photoresists were evaluated by AFM and displayed a Young's modulus range in air of 32–73 MPa and 7.44 to 18.32 MPa in water. Kelvin probe force microscopy on fabricated structures demonstrated the clear effect of incorporation of PEDOT:PSS in the photoresists, with the presence of a contact potential difference upon application of a bias in the case of the structures fabricated with photoresists 1 – PEGDA, 57.8 wt% Clevios, and 2 – PEGDA/TMPET, 58.31 wt% Clevios. Conductive-AFM measurements performed on photoresists 1 – PEGDA, 57.8 wt% Clevios and 4 – PEGDA, 20 wt% Clevios demonstrated the impact of the weight percentage of Clevios PH1000 in the formulation on the conductivity of the fabricated structures, with a 13 pA increase upon application of −5 V bias when increasing the weight content of PEDOT:PSS from 0.26 to 0.75 wt%.

DLW of PEDOT-composite microstructures can combine the advantages brought by the inclusion of the PEDOT:PSS conductive polymer with the sub-micron resolution of DLW for the realisation of 3D polymer scaffolds, where electrical stimulation and sensing together with 3D geometrical and mechanical cues can be seamlessly integrated to provide synergistic effects for cellular response and differentiation.

Conflicts of interest

There are no conflicts to declare.

Data availability

The authors declare that all data supporting the findings of this study are available within the article and its supplementary information (SI) or from the corresponding author upon reasonable request. Supplementary information is available. See DOI: https://doi.org/10.1039/d5tc02981c.

Acknowledgements

J. M. D. acknowledges support from Research Ireland through the Government of Ireland Postdoctoral Fellowship Scheme; grant number GOIPD/2022/550. L. F., S. K. and J. M. D. also acknowledge funding from the European Horizon 2020 Research and Innovation Programme (no. 899349 – 5D Nano-Printing). C. D. acknowledges funding from the European Research Council (Grant No. 101077430 – BIO4D). N. L.-L. gratefully acknowledges the support from the Spanish Ministry of Universities (FPU20/03416). M. C.-G. thanks "Ayuda RYC2022-036380-I financiada por MICIU/AEI/10.13039/5011 00011033 y por el FSE+". DLW and imaging were carried out at the Additive Research Laboratory (AR-Lab) and the Advanced Microscopy Laboratory (AML), Trinity College Dublin, Ireland. The AR-Lab and AML are part of the CRANN Institute and affiliated to the AMBER centre, funded by Research Ireland and the European Regional Development Fund (ERDF) under grant number 12/RC/2278_P2.

References

1 B. Gupta, S. Kalyan Samanta and R. Singh, *Mater. Today*, 2024, **80**, 681–709.
2 S. J. Peñas-Núñez, D. Mecerreyes and M. Criado-Gonzalez, *ACS Appl. Bio Mater.*, 2024, **7**, 7944–7964.
3 X. Zhou, P. Kateb, F. Miquet-Westphal, G. A. Lodygensky and F. Cicoira, *Adv. Sens. Res.*, 2023, **2**, 2300072.
4 X. Zhou, P. Kateb, J. Fan, J. Kim, G. A. Lodygensky, B. Amilhon, D. Pasini and F. Cicoira, *J. Mater. Chem. C*, 2024, **12**, 5708–5717.
5 S. Ahadian, J. Ramón-Azcón, M. Estili, X. Liang, S. Ostrovidov, H. Shiku, M. Ramalingam, K. Nakajima, Y. Sakka, H. Bae, T. Matsue and A. Khademhosseini, *Sci. Rep.*, 2014, **4**, 4271.
6 X. Liu, A. L. Miller II, S. Park, B. E. Waletzki, Z. Zhou, A. Terzic and L. Lu, *ACS Appl. Mater. Interfaces*, 2017, **9**, 14677–14690.
7 W. Xiong, Y. Liu, L. J. Jiang, Y. S. Zhou, D. W. Li, L. Jiang, J.-F. Silvain and Y. F. Lu, *Adv. Mater.*, 2016, **28**, 2002–2009.
8 U. Staudinger, G. Zyla, B. Krause, A. Janke, D. Fischer, C. Esen, B. Voit and A. Ostendorf, *Microelectron. Eng.*, 2017, **179**, 48–55.
9 Q. Guo, S. Xiao, A. Aumann, M. Jaeger, M. B. Chakif, R. Ghadiri, C. Esen, M. Ma and A. Ostendorf, *J. Laser Micro Nanoeng.*, 2012, **7**, 44–48.
10 S. Sayyar, E. Murray, B. C. Thompson, J. Chung, D. L. Officer, S. Gambhir, G. M. Spinks and G. G. Wallace, *J. Mater. Chem. B*, 2015, **3**, 481–490.
11 J. Yi, G. Choe, J. Park and J. Y. Lee, *Polym. J.*, 2020, **52**, 823–837.
12 M. Oubaha, A. Kavanagh, A. Gorin, G. Bickauskaite, R. Byrne, M. Farsari, R. Winfield, D. Diamond, C. McDonagh and R. Copperwhite, *J. Mater. Chem.*, 2012, **22**, 10552–10559.
13 M. Restaino, N. Eckman, A. T. Alsharhan, A. C. Lamont, J. Anderson, D. Weinstein, A. Hall and R. D. Sochol, *Adv. Mater. Technol.*, 2021, **6**, 2100222.
14 X. Jing, X.-Y. Wang, H.-Y. Mi and L.-S. Turng, *Mater. Lett.*, 2019, **237**, 53–56.
15 K. Liu, X. Pan, L. Chen, L. Huang, Y. Ni, J. Liu, S. Cao and H. Wang, *ACS Sustainable Chem. Eng.*, 2018, **6**, 6395–6403.

16 P. Baei, S. Jalili-Firoozinezhad, S. Rajabi-Zeleti, M. Tafazzoli-Shadpour, H. Baharvand and N. Aghdami, *Mater. Sci. Eng., C*, 2016, **63**, 131–141.
17 M. Criado-Gonzalez, A. Dominguez-Alfaro, N. Lopez-Larrea, N. Alegret and D. Mecerreyes, *ACS Appl. Polym. Mater.*, 2021, **3**, 2865–2883.
18 D. Won, J. Kim, J. Choi, H. Kim, S. Han, I. Ha, J. Bang, K. K. Kim, Y. Lee, T.-S. Kim, J.-H. Park, C.-Y. Kim and S. H. Ko, *Sci. Adv.*, 2022, **8**, eabo3209.
19 L. Zhou, H. Zheng, Z. Liu, S. Wang, Z. Liu, F. Chen, H. Zhang, J. Kong, F. Zhou and Q. Zhang, *ACS Nano*, 2021, **15**, 2468–2480.
20 F. Fu, J. Wang, H. Zeng and J. Yu, *ACS Mater. Lett.*, 2020, **2**, 1287–1301.
21 H. Yuk, B. Lu, S. Lin, K. Qu, J. Xu, J. Luo and X. Zhao, *Nat. Commun.*, 2020, **11**, 1604.
22 C. Liu, F. Jiang, M. Huang, R. Yue, B. Lu, J. Xu and G. Liu, *J. Electron. Mater.*, 2011, **40**, 648–651.
23 M. J. Donahue, A. Sanchez-Sanchez, S. Inal, J. Qu, R. M. Owens, D. Mecerreyes, G. G. Malliaras and D. C. Martin, *Mater. Sci. Eng., R*, 2020, **140**, 100546.
24 B. Lu, H. Yuk, S. Lin, N. Jian, K. Qu, J. Xu and X. Zhao, *Nat. Commun.*, 2019, **10**, 1043.
25 E. Bihar, T. Roberts, M. Saadaoui, T. Hervé, J. B. De Graaf and G. G. Malliaras, *Adv. Healthcare Mater.*, 2017, **6**, 1601167.
26 L.-W. Lo, J. Zhao, H. Wan, Y. Wang, S. Chakrabartty and C. Wang, *ACS Appl. Mater. Interfaces*, 2021, **13**, 21693–21702.
27 M. L. Picchio, A. Gallastegui, N. Casado, N. Lopez-Larrea, B. Marchiori, I. del Agua, M. Criado-Gonzalez, D. Mantione, R. J. Minari and D. Mecerreyes, *Adv. Mater. Technol.*, 2022, **7**, 2101680.
28 I. M. Hill, V. Hernandez, B. Xu, J. A. Piceno, J. Misiaszek, A. Giglio, E. Junez, J. Chen, P. D. Ashby, R. S. Jordan and Y. Wang, *ACS Appl. Polym. Mater.*, 2023, **5**, 3989–3998.
29 D. N. Heo, S.-J. Lee, R. Timsina, X. Qiu, N. J. Castro and L. G. Zhang, *Mater. Sci. Eng., C*, 2019, **99**, 582–590.
30 M. S. Onses, E. Sutanto, P. M. Ferreira, A. G. Alleyne and J. A. Rogers, *Small*, 2015, **11**, 4237–4266.
31 S. Lee, J.-y Kim, J. Kim, A. K. Hoshiar, J. Park, S. Lee, J. Kim, S. Pané, B. J. Nelson and H. Choi, *Adv. Healthcare Mater.*, 2020, **9**, 1901697.
32 N. Pellicciotta, O. S. Bagal, V. C. Sosa, G. Frangipane, G. Vizsnyiczai and R. D. Leonardo, *Adv. Funct. Mater.*, 2023, **33**, 2214801.
33 A. Augustine, J. Qian, T. Faraone, S. Kolagatla, N. Prochukhan, M. A. Morris, A. L. Bradley, L. Florea and C. Delaney, *Small*, 2024, **20**, 2310058.
34 C. Delaney, J. Qian, X. Zhang, R. Potyrailo, A. L. Bradley and L. Florea, *J. Mater. Chem. C*, 2021, **9**, 11674–11678.
35 J. Qian, S. Kolagatla, A. Pacalovas, X. Zhang, L. Florea, A. L. Bradley and C. Delaney, *Adv. Funct. Mater.*, 2023, **33**, 2211735.
36 A. Ennis, D. Nicdao, S. Kolagatla, L. Dowling, Y. Tskhe, A. J. Thompson, D. Trimble, C. Delaney and L. Florea, *Adv. Funct. Mater.*, 2023, **33**, 2213947.
37 S. Rani, R. K. Das, A. Jaiswal, G. P. Singh, A. Palwe, S. Saxena and S. Shukla, *Chem. Eng. J.*, 2023, **454**, 140130.
38 R. Wollhofen, M. Axmann, P. Freudenthaler, C. Gabriel, C. Röhrl, H. Stangl, T. A. Klar and J. Jacak, *ACS Appl. Mater. Interfaces*, 2018, **10**, 1474–1479.
39 J. Li, P. Fejes, D. Lorenser, B. C. Quirk, P. B. Noble, R. W. Kirk, A. Orth, F. M. Wood, B. C. Gibson, D. D. Sampson and R. A. McLaughlin, *Sci. Rep.*, 2018, **8**, 14789.
40 M. Marini, A. Nardini, R. Martínez Vázquez, C. Conci, M. Bouzin, M. Collini, R. Osellame, G. Cerullo, B. S. Kariman, M. Farsari, E. Kabouraki, M. T. Raimondi and G. Chirico, *Adv. Funct. Mater.*, 2023, **33**, 2213926.
41 S. Donato, S. Nocentini, D. Martella, S. Kolagatla, D. S. Wiersma, C. Parmeggiani, C. Delaney and L. Florea, *Small*, 2024, **20**, 2306802.
42 M. del Pozo, C. Delaney, M. Pilz da Cunha, M. G. Debije, L. Florea and A. P. H. J. Schenning, *Small Struct.*, 2022, **3**, 2100158.
43 J.-Y. Wang, F. Jin, X.-Z. Dong, J. Liu and M.-L. Zheng, *Adv. Mater. Technol.*, 2022, **7**, 2200276.
44 Z.-C. Ma, Y.-L. Zhang, B. Han, X.-Y. Hu, C.-H. Li, Q.-D. Chen and H.-B. Sun, *Nat. Commun.*, 2020, **11**, 4536.
45 E. D. Lemma, S. Sergio, B. Spagnolo, M. Pisanello, L. Algieri, M. A. Coluccia, M. Maffia, M. De Vittorio and F. Pisanello, *Microelectron. Eng.*, 2018, **190**, 11–18.
46 J. Song, C. Michas, C. S. Chen, A. E. White and M. W. Grinstaff, *Adv. Healthcare Mater.*, 2020, **9**, 1901217.
47 L. Yang, H. Hu, A. Scholz, F. Feist, G. Cadilha Marques, S. Kraus, N. M. Bojanowski, E. Blasco, C. Barner-Kowollik, J. Aghassi-Hagmann and M. Wegener, *Nat. Commun.*, 2023, **14**, 1103.
48 E. Blasco, J. Müller, P. Müller, V. Trouillet, M. Schön, T. Scherer, C. Barner-Kowollik and M. Wegener, *Adv. Mater.*, 2016, **28**, 3592–3595.
49 C. Kindle, A. Castonguay, S. McGee, J. A. Tomko, P. E. Hopkins and L. D. Zarzar, *ACS Appl. Nano Mater.*, 2019, **2**, 2581–2586.
50 S. Shukla, X. Vidal, E. P. Furlani, M. T. Swihart, K.-T. Kim, Y.-K. Yoon, A. Urbas and P. N. Prasad, *ACS Nano*, 2011, **5**, 1947–1957.
51 S. Maruo and T. Saeki, *Opt. Express*, 2008, **16**, 1174–1179.
52 X. Zhou, X. Liu and Z. Gu, *Adv. Mater.*, 2024, **36**, 2409326.
53 Y. Tao, C. Wei, J. Liu, C. Deng, S. Cai and W. Xiong, *Nanoscale*, 2019, **11**, 9176–9184.
54 K. Kurselis, R. Kiyan, V. N. Bagratashvili, V. K. Popov and B. N. Chichkov, *Opt. Express*, 2013, **21**, 31029–31035.
55 C. Amruth, A. K. Singh, A. Sharma, D. Corzo and D. Baran, *Adv. Mater. Technol.*, 2024, **9**, 2400290.
56 O. Dadras-Toussi, M. Khorrami, A. S. C. Louis Sam Titus, S. Majd, C. Mohan and M. R. Abidian, *Adv. Mater.*, 2022, **34**, 2200512.
57 K. M. Lichade, S. Shiravi, J. D. Finan and Y. Pan, *Addit. Manuf.*, 2024, **84**, 104123.
58 A. Selimis, V. Mironov and M. Farsari, *Microelectron. Eng.*, 2015, **132**, 83–89.
59 S. Garreau, G. Louarn, J. P. Buisson, G. Froyer and S. Lefrant, *Macromolecules*, 1999, **32**, 6807–6812.

60 L. J. Jiang, Y. S. Zhou, W. Xiong, Y. Gao, X. Huang, L. Jiang, T. Baldacchini, J.-F. Silvain and Y. F. Lu, *Opt. Lett.*, 2014, **39**, 3034–3037.
61 M. B. Moran and G. C. Martin, *J. Macromol. Sci., Part A: Pure Appl. Chem.*, 1983, **19**, 611–618.
62 G. Socrates, *Infrared and Raman characteristic group frequencies: tables and charts*, John Wiley & Sons, 2004.
63 Z. Fan, D. Du, H. Yao and J. Ouyang, *ACS Appl. Mater. Interfaces*, 2017, **9**, 11732–11738.
64 W. Melitz, J. Shen, A. C. Kummel and S. Lee, *Surf. Sci. Rep.*, 2011, **66**, 1–27.
65 Z. Li, Y. Liang, Z. Zhong, J. Qian, G. Liang, K. Zhao, H. Shi, S. Zhong, Y. Yin and W. Tian, *Synth. Met.*, 2015, **210**, 363–366.